Stability of the spiral spin liquid in $MnSc_2S_4$

Yasir Iqbal,[1] Tobias Müller,[2] Harald O. Jeschke,[3] Ronny Thomale,[2] and Johannes Reuther[4,5]

[1]*Department of Physics, Indian Institute of Technology Madras, Chennai 600036, India*
[2]*Institute for Theoretical Physics and Astrophysics, Julius-Maximilian's University of Würzburg, Am Hubland, D-97074 Würzburg, Germany*
[3]*Research Institute for Interdisciplinary Science, Okayama University, 3-1-1 Tsushima-naka, Kita-ku, Okayama 700-8530, Japan*
[4]*Dahlem Center for Complex Quantum Systems and Institut für Theoretische Physik, Freie Universität Berlin, Arnimallee 14, 14195 Berlin, Germany*
[5]*Helmholtz-Zentrum für Materialien und Energie, Hahn-Meitner-Platz 1, 14019 Berlin, Germany*

(Dated: February 2, 2018)

We investigate the stability of the spiral spin-liquid phase in $MnSc_2S_4$ against thermal and quantum fluctuations as well as against perturbing effects of longer-range interactions. Employing *ab initio* DFT calculations we propose a realistic Hamiltonian for $MnSc_2S_4$, featuring second (J_2) and third (J_3) neighbor Heisenberg interactions on the diamond lattice that are considerably larger than previously assumed. We argue that the combination of strong J_2 and J_3 couplings reproduces the correct magnetic Bragg peak position measured experimentally. Calculating the spin-structure factor within the pseudofermion functional-renormalization group technique we find that close to the magnetic phase transition the sizeable J_3 couplings induce a strong spiral selection effect, in agreement with experiments. With increasing temperature the spiral selection becomes weaker such that around three times the ordering temperature an approximate spiral spin-liquid is realized in $MnSc_2S_4$.

Introduction. If magnetic frustration is sufficiently strong, a spin system may evade spontaneous symmetry breaking at low temperatures and instead form a highly entangled state where the spins fluctuate in a cooperative manner. This so-called spin liquid state generally exists in two different flavors – the quantum [1–3] and the classical spin liquid [4–7]. The first case preferably occurs for small quantum spins in combination with frustrated lattice geometries and/or anisotropic interactions where quantum fluctuations may reach the size of the local spin magnitude thus hindering the system from developing magnetic long-range order. In the second case, spin liquid-like behavior even survives in the complete absence of quantum fluctuations such as for classical ($S \to \infty$) spins. The suppression of long-range magnetic order now relies on a macroscopic degeneracy of classical ground states through which the system fluctuates collectively, thus justifying the notion of a classical spin liquid. Paradigmatic examples are pyrochlore spin-ice systems [4, 5] where at zero temperature an ice rule (e.g., the famous two-in-two-out rule) imposes local constraints on possible spin states. Since these rules leave the ground-state spin configuration underdetermined, the system maintains a macroscopic (extensive) classical degeneracy [8].

Interestingly, for certain lattice geometries and special arrangements of frustrating interactions, classical spin liquids even exist without a local ice-rule constraint. This rare situation is realized on the three-dimensional diamond lattice [Fig. 1(a)] with first (J_1) and second (J_2) neighbor Heisenberg interactions where $\frac{J_2}{|J_1|} > \frac{1}{8}$ and J_2 must be antiferromagnetic [6, 9–11]. The competing interactions force the system into classical coplanar spin-spirals. Remarkably, the ground state is formed from a highly degenerate set of such spirals where the corresponding wave vectors $\mathbf{q}$ occupy a closed surface in reciprocal space (note that a similar scenario also occurs on the two-dimensional honeycomb lattice [12–14]). Due to the cooperative motion of spins through the degenerate manifold of spirals, this state has been dubbed a *spiral spin-liquid*.

Spiral spin-liquids are generally very fragile to perturbations of various different types. Any finite additional term in the Hamiltonian such as third neighbor couplings J_3 or dipolar interactions typically selects specific spirals out of the degenerate manifold and consequently generate long-range magnetic order. Even in the absence of such perturbations, a lifting of the degeneracy takes place due to thermal fluctuations, i.e., a finite temperature transition into a magnetically ordered state is induced by an entropic "order-by-disorder" selection [15] of spirals. As has been found in Ref. [6], by varying $\frac{J_2}{|J_1|} > \frac{1}{8}$ the system goes through a sequence of different magnetic phases. While strictly speaking this effect destroys spiral spin-liquids at any finite temperature, an approximate version of this state may still survive in a temperature range *above* the transition where the thermal selection is not yet active. Finally, quantum fluctuations at large but finite spin magnitudes have been found to induce an order-by-disorder effect similar to thermal fluctuations [11].

Currently, the most promising material to approximately realize a spiral spin-liquid is the A-site spinel $MnSc_2S_4$ [7, 16–20] where spin-5/2 Mn^{2+} ions occupy the sites of a diamond lattice. At ~ 2.9 K which is well below the Curie-Weiss temperature of $|\Theta_{\rm CW}| = 23$ K [16] but still inside the paramagnetic phase of this compound (which survives down to ~ 2.3 K [7, 16, 18–20]) neutron scattering directly observes surface-like scattering profiles in momentum space, reminiscent of a spiral spin-liquid [7]. From the radius of this surface a coupling ratio of $\frac{J_2}{|J_1|} = 0.85$ has been determined [6] (where J_1 is ferromagnetic). The measured spin-structure factor is not evenly distributed on the spiral surface but shows higher intensities for spirals with wave vectors $\mathbf{q} \sim 2\pi(0.75, 0.75, 0)$ and symmetry-related positions [7, 18, 20]. This spiral selection turns into real magnetic long-range order below $T_c = 2.3$ K [18, 20] (other works report slightly smaller values of $T_c \approx 2.1$ K [7, 16, 19]). It is worth emphasizing that this peak position does not coincide with the thermal selection

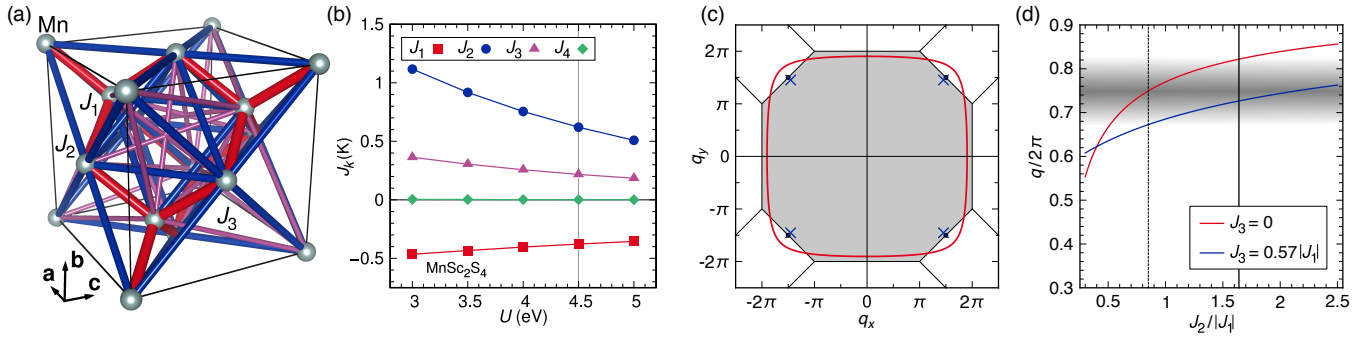

FIG. 1. (a) Cubic unit cell of the diamond lattice with first (J_1), second (J_2), and third (J_3) neighbor couplings. (b) Couplings J_1–J_4 from DFT as a function of the Hubbard U interaction. The vertical line indicates the exchange couplings investigated in the main text. (c) Classical spin-spiral surface in the q_x–q_y plane for $J_2/|J_1| = 1.64$ and $J_3 = 0$ (red line). The blue crosses indicate the Bragg peak position for an additional third neighbor coupling $J_3/|J_1| = 0.57$. Black dots highlight the measured magnetic order at $\mathbf{q} \sim 2\pi(0.75, 0.75, 0)$. (d) Red: Size of the spiral surface [given by the intersection with the line $(q, q, 0)$] as a function of J_2 and for $J_3 = 0$. Blue: $(q, q, 0)$-position of the ordering wave vector for $J_3/|J_1| = 0.57$. Vertical full (dashed) lines indicate the coupling ratios $J_2/|J_1| = 1.64$ ($J_2/|J_1| = 0.85$ [6]). The shaded area marks the position and width of the measured magnetic Bragg peak $\mathbf{q} \sim 2\pi(0.75, 0.75, 0)$ [7].

predicted in Ref. [6] but rather points towards the presence of longer-range J_3 interactions.

This Rapid Communication complements recent experimental works by theoretically investigating the fate of the spiral spin-liquid when assuming a realistic model for $MnSc_2S_4$. To this end, we first employ *ab initio* DFT calculations to determine the microscopic Hamiltonian of this compound. We then treat the resulting model within the pseudofermion functional renormalization group (PFFRG) method [21] which is capable of resolving the effects of thermal and quantum fluctuations, and we clarify the role of third neighbor J_3 interactions. In particular, we investigate to which degree the spiral spin-liquid phase in $MnSc_2S_4$ remains stable under such perturbations and compare the $\mathbf{q}$-space resolved magnetic susceptibility with neutron scattering experiments. Our main results are summarized as follows: (i) We find that the J_2 and J_3 interactions are both considerably larger than previously assumed, (ii) Close to the magnetic phase transition but still inside the paramagnetic regime the spin correlations are dominated by J_3 couplings which induce a pronounced selection of spirals with wave vectors $\mathbf{q} \approx 2\pi(0.72, 0.72, 0)$, in excellent agreement with experiments, (iii) We identify a temperature regime around $3T_c$ where the spiral selection due to J_3 couplings is suppressed such that the system realizes an approximate spiral spin-liquid, and (iv) PFFRG calculations for our model Hamiltonian reproduce the measured spin structure factor for $MnSc_2S_4$ with remarkable accuracy.

Methods. We base our calculations on the cubic spinel structure determined by neutron powder diffraction at $T = 1.6$ K [18]. The Mn^{2+} ions form a diamond lattice as shown in Fig. 1(a). We use an energy mapping techique to determine the most important exchange interactions in $MnSc_2S_4$ [22–24]. For this purpose we construct a $2 \times 2 \times 1$ supercell of the original primitive cell containing two Mn^{2+} ions; in $P\,m$ space group, this supercell has eight inequivalent Mn sites allowing for 20 distinct spin configurations. This allows us to determine the first four exchange couplings, extending up to a Mn–Mn distance of 10.6 Å. We perform density functional theory calculations with the all electron full potential local orbital (FPLO) [25] basis set and generalized gradient approximation (GGA) [26] exchange correlation functional, accounting for the strong correlations on the Mn $3d$ orbitals by a GGA+U [27] correction. The Hunds rule coupling for Mn $3d$ was fixed at $J_H = 0.76$ eV [28]. The result of fitting the DFT total energies against the Heisenberg Hamiltonian

$$\hat{\mathcal{H}} = \sum_{k=1}^{4} \sum_{\langle ij \rangle_k} J_k \hat{\mathbf{S}}_i \cdot \hat{\mathbf{S}}_j \,, \tag{1}$$

where $\langle ij \rangle_k$ denotes pairs of kth neighbor sites on the diamond lattice is shown in Fig. 1(b) and Table S1 for five values of the interaction strength U [29]. As explained below, the value of U is fixed by the experimentally observed Curie-Weiss temperature Θ_{CW}.

The spin Hamiltonian from DFT is taken as an input for the PFFRG method [21]. To treat this model within standard many-body techniques, the PFFRG first expresses the spin operators in terms of Abrikosov pseudofermions [30]. The implementation of the local spin-5/2 moments is performed as described in Ref. [14] where multiple copies of spin-1/2 degrees of freedom effectively realize spins with larger magnitudes. The resulting fermionic Hamiltonian is then investigated using the well-developed FRG method [31, 32], which calculates the evolution of m-particle vertices as a function of an RG parameter Λ. Effectively, the vertex flow takes into account leading diagrammatic contributions in $1/S$ [14] and $1/N$ [33, 34], such that classical spin correlations and quantum fluctuations (described in large S and large N approaches, respectively) are both faithfully captured. After its initial development in two dimensions [21], the PFFRG has been further refined and applied to various models of frustrated magnetism including multi-layer, and, eventually, three-dimensional magnets [11, 14, 24, 33–47]. The finite size approximation in the PFFRG amounts to limiting the real-space distance of spin correlations, which in our calculations extends over 12 nearest neighbor lattice spacings, correspond-

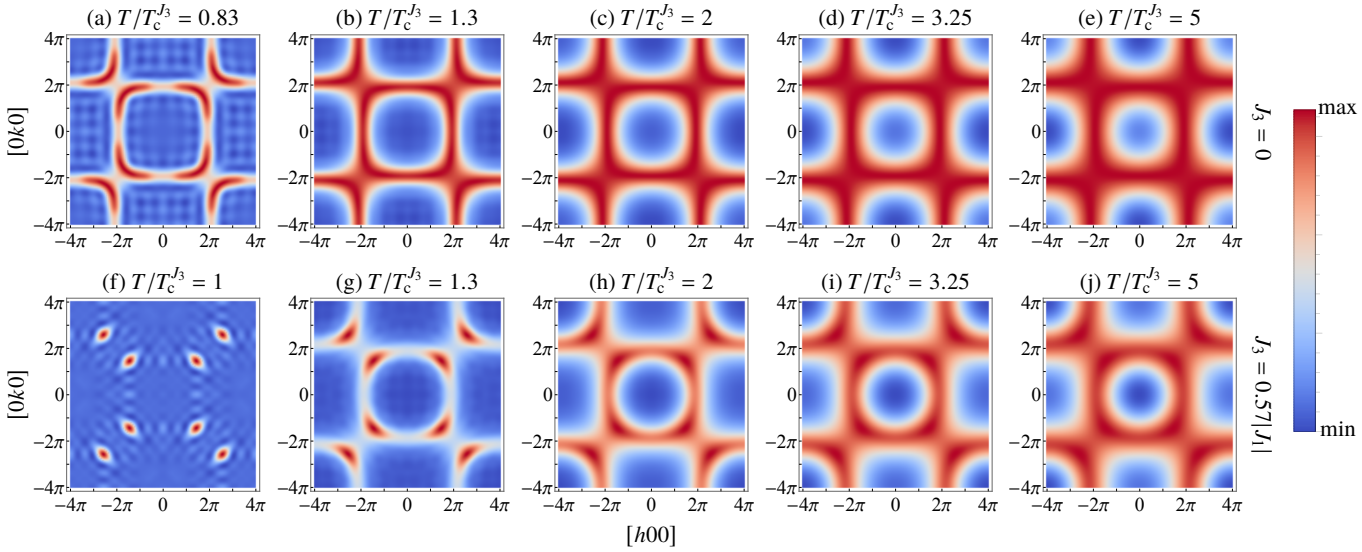

FIG. 2. The evolution of the spin susceptibility (in units of $1/|J_1|$) profile in the q_x–q_y plane with temperature for the Heisenberg Hamiltonian of $MnSc_2S_4$ as determined from DFT. (a)–(e) Evaluated for a J_1–J_2 *only* model with $J_2/|J_1| = 1.64$ and $J_3 = 0$, (f)–(j) Evaluated for the full J_1–J_2–J_3 Hamiltonian with $J_2/|J_1| = 1.64$ and $J_3/|J_1| = 0.57$. The temperatures are expressed in units of the critical (ordering) temperature $T_c^{J_3}$ of the full model Hamiltonian with $J_3/|J_1| = 0.57$. For each of the above profiles, the variation of the susceptibility along the $(q, q, 0)$ $1D$ cut is shown in Fig. S2.

ing to a correlation volume of 1963 sites. Likewise, the continuous frequency arguments of the vertex functions are approximated by a discrete set of 64 frequencies. The central physical quantity studied within the PFFRG is the static (zero-frequency) momentum-resolved susceptibility (or spin structure factor) which can be directly compared with experimental neutron scattering data.

Model Hamiltonian and classical considerations. We first discuss the exchange couplings J_k in Eq. (1) determined from DFT. As shown in Fig. 1(b), DFT calculates these couplings as a function of the Hubbard onsite interaction U. Upon increasing U, all couplings decrease but their ratios remain relatively constant. The actual size of U is determined via the known Curie-Weiss temperature $\Theta_{\rm CW} = -\frac{S(S+1)}{3k_B}\sum_{k=1}^{4} z_k J_k = -23$ K [16] (where z_k is the coordination number of the kth neighbor bonds). This condition is best fulfilled for $U \approx 4.5$ eV, yielding three significant couplings $J_1 = -0.378$ K, $J_2 = 0.621$ K, $J_3 = 0.217$ K, and $J_4 = 0.0015$ K. Since J_4 is more than an order of magnitude smaller than all other couplings it will be neglected in the ensuing analysis.

The DFT couplings might first appear unexpected because the ratios $\frac{J_2}{|J_1|} = 1.64$ and $\frac{J_3}{|J_1|} = 0.57$ are considerably larger compared to the values $\frac{J_2}{|J_1|} \approx 0.85$ and $\frac{J_3}{|J_1|} \lesssim 0.1$ proposed earlier (see Refs. [6, 9], respectively). To shed further light on the physical implications of these new couplings we first treat Eq. (1) within the classical Luttinger-Tisza method [48, 49] which relaxes the spins' length constraint (note that for a diamond-lattice geometry this soft-spin approach even becomes exact, see Supplementary Material for further details). Ignoring J_3 for a moment, the J_1–J_2 only model with $\frac{J_2}{|J_1|} = 1.64$ exhibits a spiral surface in momentum space which cuts through the first Brillouin-zone boundary [see Fig. 1(c)]. This surface is slightly larger than the one for $\frac{J_2}{|J_1|} = 0.85$, where the latter ratio has been determined in Ref. [6] to match the measured magnetic Bragg peak position $\mathbf{q} \approx 2\pi(0.75, 0.75, 0)$ for $J_3 = 0$. Although the spiral surface only undergoes a moderate increase between $\frac{J_2}{|J_1|} = 0.85$ and $\frac{J_2}{|J_1|} = 1.64$, the DFT couplings first seem to overestimate the ordering wave vector even when the finite Bragg-peak width is taken into account [see Fig. 1(d)]. The situation changes when J_3 couplings are considered. Already an infinitesimally small J_3 lifts the degeneracy and selects spirals with $\mathbf{q} = (q, q, 0)$ along the surface. For larger (antiferromagnetic) J_3 this Bragg-peak position moves inwards in $\mathbf{q}$ space. As shown in Figs. 1(c) and (d), the third neighbor coupling $\frac{J_3}{|J_1|} = 0.57$ from DFT indeed shifts the Bragg-peak back to $\mathbf{q} = 2\pi(0.73, 0.73, 0)$ in very good agreement with the measured position. As discussed in Ref. [9], small remaining discrepancies might disappear when incommensurate/commensurate "lock-in" transitions are considered.

PFFRG results. Having argued that our model parameters are generally compatible with the experimental findings, we next investigate to which extent the strong J_3 coupling together with thermal and quantum fluctuations destabilize the spiral spin-liquid. To this end, we first calculate the spin-structure factor via PFFRG for $\frac{J_2}{|J_1|} = 1.64$ and $J_3 = 0$ where only the effects of thermal and quantum fluctuations lift the spiral degeneracy [see Figs. 2(a)–(e)], and then compare with $\frac{J_3}{|J_1|} = 0.57$, to study the additional influence of third neighbor coupling [see Figs. 2(f)–(j)]. In both cases, the spin-structure factor is investigated as a function of the RG parameter Λ which has been argued to mimic finite temperatures T [36, 38, 46] [50].

For $J_3 = 0$ and at the critical RG scale (which corre-

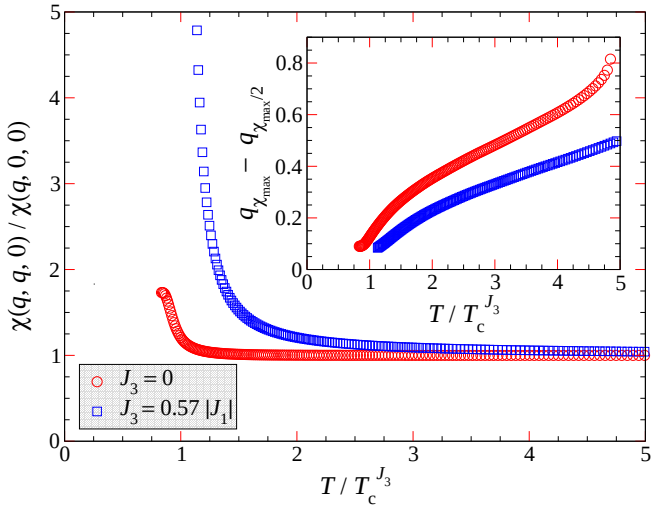

FIG. 3. The ratio of the susceptibility maxima along the $(q, q, 0)$ and $(q, 0, 0)$-directions shown as a function of temperature T. (Inset) Temperature evolution of the width of the spiral surface along the $(q, q, 0)$-direction. The width is defined as the difference of the q-values for the maxima and half-maxima of the susceptibility, respectively.

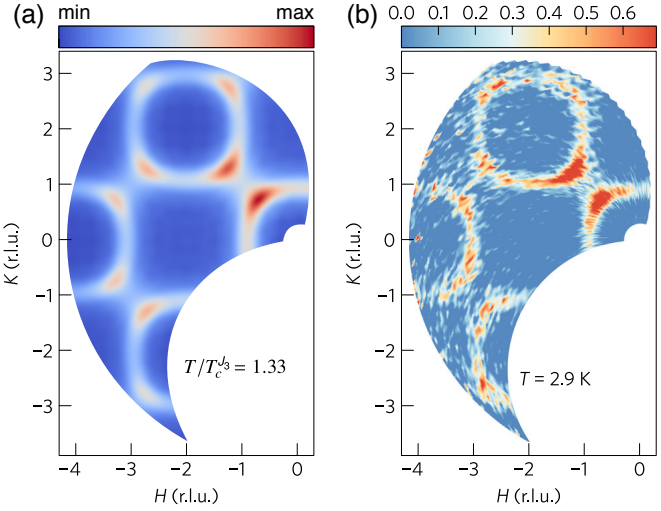

FIG. 4. Calculated (a) and measured (b) spin-structure factor in the q_x–q_y plane for $T/T_c^{J_3} = 1.33$ and $T = 2.9$ K, respectively [(b) has been reproduced from Ref. [7]].

sponds to $\Lambda_c^0 = 0.83(1)|J_1|$) the PFFRG detects a sharp spiral contour of strong intensities. Along finite segments centered around $(q, q, 0)$ we find somewhat larger (and nearly constant) responses, however, this modulation quickly disappears with increasing temperature (i.e., RG scale Λ) such that an almost perfect spiral surface appears. Furthermore, the size and shape of the spiral surface remains nearly constant as a function of temperature [see Fig. S1(a)] while its width increases [see inset of Fig. 3]. A more quantitative measure for the intactness of the spiral surface is shown in Fig. 3 where the ratio of the intensity maximum along the $(q, q, 0)$ and along the $(q, 0, 0)$ direction is plotted. This quantity approaches $\chi(q, q, 0)/\chi(q, 0, 0) \approx 1$ around $\Lambda \approx 2\Lambda_c^0$ indicating that the spiral surface quickly recovers. We also note that compared to our classical Luttinger-Tisza analysis, the location of the spiral surface does not undergo any noticeable changes when including quantum fluctuations.

Switching on the third neighbor coupling $\frac{J_3}{|J_1|} = 0.57$ induces a much stronger spiral-selection effect. At criticality, we observe pronounced peaks at $\mathbf{q} = 2\pi(0.719, 0.719, 0)$ [see Fig. 2(f)] which are found to be slightly shifted inwards compared to the classical wave-vector position $\mathbf{q} = 2\pi(0.727, 0.727, 0)$. The critical RG scale $\Lambda_c^{J_3} = 0.99(1)|J_1|$ is slightly larger compared to the one for $J_3 = 0$, indicating that third neighbor interactions *reduce* the frustration. With increasing temperature, the response again becomes more evenly distributed along the spiral surface, however, this intensity smearing occurs more slowly than for $J_3 = 0$. This is also seen in Fig. 3 where the ratio of the maxima along $(q, q, 0)$ and $(q, 0, 0)$ starts with a large (diverging) value at $\Lambda_c^{J_3}$ and then slowly converges towards one. Yet, around $\Lambda \approx 3\Lambda_c^{J_3}$ we observe a temperature regime where the surface is relatively intact. Interestingly, the width of the spiral surface is also seen to decrease upon inclusion of a J_3 coupling [see inset of Fig. 3] implying that the response is concentrated within a narrower stripe around the spiral surface compared to the case with $J_3 = 0$, leading to a well-defined and "intact" spiral spin-liquid. These results indicate that at temperatures about three times the size of the ordering temperature of $T_c = 2.3$ K (which is still much smaller than the Curie-Weiss temperature) $MnSc_2S_4$ indeed realizes an approximate spiral spin-liquid.

Finally, to directly assess the quality of our simulations, we compare the measured spin structure-factor at $T = 2.9$ K $= 1.33T_c$ [7] with the PFFRG result for the full DFT model at the same RG-scale ratio $\Lambda = 1.33\Lambda_c^{J_3}$, see Fig. 4 (note that in contrast to Fig. 2 this plot also takes into account the magnetic form factor of Mn^{2+} ions which suppresses the spin structure-factor at large $|\mathbf{q}|$). As can be seen, the measured intensity modulation and, in particular, the spiral selection (which is still pronounced at these temperatures) is nicely reproduced by our calculations.

Discussion and conclusion. By combining *ab initio* DFT and PFFRG calculations we have shown that close to criticality the magnetic ordering process of $MnSc_2S_4$ is dominated by a pronounced $(q, q, 0)$-spiral selection due to strong J_3 couplings. Yet, as temperature increases, thermal fluctuations largely restore the spiral surface such that an approximate version of a spiral spin-liquid is realized at around three times the ordering temperature. Interestingly, we find that the J_3 coupling is not entirely detrimental to a spiral spin-liquid, since the selection induced by such interactions is accompanied by a reduction of the spiral surface's width.

While the Heisenberg couplings considered here determine the momentum structure of the spin correlations, they leave the plane of spiral rotation undetermined. This remaining degeneracy may be further lifted by anisotropic interactions such as dipolar couplings [7, 9]. However, with a magnitude of a few percent of J_1 (Ref. [7] gives an estimate of ~ 0.026 K

on nearest neighbor bonds) we expect dipolar interactions to become relevant only very close to the ordering transition. On the other hand, *below* criticality such couplings might be crucial for explaining the measured multistep ordering process involving sinusoidal collinear, incommensurate, and helical spin orders [7]. Since the PFFRG in its current formulation does not explicitly take into account spontaneous symmetry breaking, an analysis of such phases goes beyond the scope of the present work.

Acknowledgements. Y.I. and R.T. gratefully acknowledge the Gauss Centre for Supercomputing e.V. for funding this project by providing computing time on the GCS Supercomputer SuperMUC at Leibniz Supercomputing Centre (LRZ). The work in Würzburg has been supported by ERC-StG-Thomale-336012, DFG-SFB 1170, and DFG-SPP 1666. J.R. is supported by the Freie Universität Berlin within the Excellence Initiative of the German Research Foundation.

[1] P. Anderson, Mater. Res. Bull. **8**, 153 (1973).
[2] L. Balents, Nature (London) **464**, 199 (2010).
[3] L. Savary and L. Balents, Rep. Prog. Phys. **80**, 016502 (2017).
[4] A. P. Ramirez, A. Hayashi, R. J. Cava, R. Siddharthan, and B. S. Shastry, Nature (London) **399**, 333 (1999).
[5] S. T. Bramwell and M. J. P. Gingras, Science **294**, 1495 (2001).
[6] D. Bergman, J. Alicea, E. Gull, S. Trebst, and L. Balents, Nat. Phys. **3**, 487 (2007).
[7] S. Gao, O. Zaharko, V. Tsurkan, Y. Su, J. S. White, G. S. Tucker, B. Roessli, F. Bourdarot, R. Sibille, D. Chernyshov, T. Fennell, A. Loidl, and C. Rüegg, Nat. Phys. **13**, 157 (2016).
[8] L. Pauling, J. Am. Chem. Soc. **57**, 2680 (1935).
[9] S. Lee and L. Balents, Phys. Rev. B **78**, 144417 (2008).
[10] L. Savary, E. Gull, S. Trebst, J. Alicea, D. Bergman, and L. Balents, Phys. Rev. B **84**, 064438 (2011).
[11] F. L. Buessen, M. Hering, J. Reuther, and S. Trebst, Phys. Rev. Lett. **120**, 057201 (2018).
[12] J. Fouet, P. Sindzingre, and C. Lhuillier, Eur. Phys. J. B **20**, 241 (2001).
[13] A. Mulder, R. Ganesh, L. Capriotti, and A. Paramekanti, Phys. Rev. B **81**, 214419 (2010).
[14] M. L. Baez and J. Reuther, Phys. Rev. B **96**, 045144 (2017).
[15] J. Villain, R. Bidaux, J.-P. Carton, and R. Conte, J. Phys. France **41**, 1263 (1980).
[16] V. Fritsch, J. Hemberger, N. Büttgen, E.-W. Scheidt, H.-A. Krug von Nidda, A. Loidl, and V. Tsurkan, Phys. Rev. Lett. **92**, 116401 (2004).
[17] S. Giri, H. Nakamura, and T. Kohara, Phys. Rev. B **72**, 132404 (2005).
[18] A. Krimmel, M. Mücksch, V. Tsurkan, M. M. Koza, H. Mutka, C. Ritter, D. V. Sheptyakov, S. Horn, and A. Loidl, Phys. Rev. B **73**, 014413 (2006).
[19] G. Kalvius, O. Hartmann, D. Noakes, F. Wagner, R. Wppling, U. Zimmermann, C. Baines, A. Krimmel, V. Tsurkan, and A. Loidl, Physica B **378-380**, 592 (2006).
[20] M. Mücksch, M. M. Koza, H. Mutka, C. Ritter, A. Cervellino, A. Podlesnyak, D. Sheptyakov, V. Tsurkan, A. Krimmel, S. Horn, and A. Loidl, J. Phys. Condens. Matter **19**, 145262 (2007).
[21] J. Reuther and P. Wölfle, Phys. Rev. B **81**, 144410 (2010).
[22] H. O. Jeschke, F. Salvat-Pujol, and R. Valentí, Phys. Rev. B **88**, 075106 (2013).
[23] D. Guterding, R. Valentí, and H. O. Jeschke, Phys. Rev. B **94**, 125136 (2016).
[24] Y. Iqbal, T. Müller, K. Riedl, J. Reuther, S. Rachel, R. Valentí, M. J. P. Gingras, R. Thomale, and H. O. Jeschke, Phys. Rev. Materials **1**, 071201 (2017).
[25] K. Koepernik and H. Eschrig, Phys. Rev. B **59**, 1743 (1999).
[26] J. P. Perdew, K. Burke, and M. Ernzerhof, Phys. Rev. Lett. **77**, 3865 (1996).
[27] A. I. Liechtenstein, V. I. Anisimov, and J. Zaanen, Phys. Rev. B **52**, R5467 (1995).
[28] T. Mizokawa and A. Fujimori, Phys. Rev. B **54**, 5368 (1996).
[29] Each pair of sites in the summation of Eq. (1) is accounted for only once, i.e., we adopt the convention of single-counting of bonds.
[30] A. A. Abrikosov, Physics (Long Island City, NY) **2**, 5 (1965).
[31] W. Metzner, M. Salmhofer, C. Honerkamp, V. Meden, and K. Schönhammer, Rev. Mod. Phys. **84**, 299 (2012).
[32] C. Platt, W. Hanke, and R. Thomale, Adv. Phys **62**, 453 (2013).
[33] F. L. Buessen, D. Roscher, S. Diehl, and S. Trebst, arXiv:1711.02182 (2017).
[34] D. Roscher, F. L. Buessen, M. M. Scherer, S. Trebst, and S. Diehl, arXiv:1711.02183 (2017).
[35] C. Balz, B. Lake, J. Reuther, H. Luetkens, R. Schönemann, T. Herrmannsdörfer, Y. Singh, A. T. M. Nazmul Islam, E. M. Wheeler, J. A. Rodriguez-Rivera, T. Guidi, G. G. Simeoni, C. Baines, and H. Ryll, Nat. Phys. **12**, 942 (2016).
[36] Y. Iqbal, R. Thomale, F. Parisen Toldin, S. Rachel, and J. Reuther, Phys. Rev. B **94**, 140408 (2016).
[37] Y. Iqbal, H. O. Jeschke, J. Reuther, R. Valentí, I. I. Mazin, M. Greiter, and R. Thomale, Phys. Rev. B **92**, 220404 (2015).
[38] J. Reuther, R. Thomale, and S. Trebst, Phys. Rev. B **84**, 100406 (2011).
[39] J. Reuther and R. Thomale, Phys. Rev. B **83**, 024402 (2011).
[40] J. Reuther, D. A. Abanin, and R. Thomale, Phys. Rev. B **84**, 014417 (2011).
[41] Y. Singh, S. Manni, J. Reuther, T. Berlijn, R. Thomale, W. Ku, S. Trebst, and P. Gegenwart, Phys. Rev. Lett. **108**, 127203 (2012).
[42] J. Reuther and R. Thomale, Phys. Rev. B **89**, 024412 (2014).
[43] R. Suttner, C. Platt, J. Reuther, and R. Thomale, Phys. Rev. B **89**, 020408 (2014).
[44] Y. Iqbal, P. Ghosh, R. Narayanan, B. Kumar, J. Reuther, and R. Thomale, Phys. Rev. B **94**, 224403 (2016).
[45] Y. Iqbal, W.-J. Hu, R. Thomale, D. Poilblanc, and F. Becca, Phys. Rev. B **93**, 144411 (2016).
[46] F. L. Buessen and S. Trebst, Phys. Rev. B **94**, 235138 (2016).
[47] A. Keles and E. Zhao, arXiv:1801.00842 (2018).
[48] J. M. Luttinger and L. Tisza, Phys. Rev. **70**, 954 (1946).
[49] J. M. Luttinger, Phys. Rev. **81**, 1015 (1951).
[50] The conversion factor between the RG scale Λ and temperature T evaluates to $\frac{T}{J} = \left(\frac{2\pi S(S+1)}{3}\right)\frac{\Lambda}{J}$. This is determined by comparing the limit of PFFRG where only the RPA diagrams contribute, i.e., a mean-field description, and the conventional spin mean-field theory formulated in terms of temperature T instead of Λ.

—Supplemental Material—
Stability of the spiral spin liquid in $MnSc_2S_4$

Luttinger-Tisza method. The Luttinger-Tisza method aims at calculating the ground state of the classical limit of the Heisenberg model by minimizing the energy given by Eq. (1), where the spin operators are substituted by classical continuous normalized vectors. To this end, the normalization of the spin vectors is replaced by the *weak constraint* that the normalization only holds on average in a given spin configuration. This permits to decompose the spin system into its Fourier modes, which is done on the two FCC sublattices of the diamond lattice separately, leading to an interaction matrix in Fourier space

$$\tilde{J}_{\alpha\beta}(\mathbf{k}) = \sum_{i,j} J_k e^{i\mathbf{k}\cdot\mathbf{R}_{\alpha,i;\beta,j}}, \tag{S1}$$

where $\mathbf{R}_{\alpha,i;\beta,j}$ is the vector connecting site i in the FCC sublattice α and site j in the FCC sublattice β, which are kth neighbors to each other. The ground state subject to the weak constraint is subsequantly given by the wavevectors $\mathbf{k}$, where the lowest eigenvalue of Eq. (S1) has its minimum. The corresponding eigenvector gives the relative weight of the mode on the sublattices, which has to have the same absolute value for a configuration to also satisfy the strong normalization constraint. As in the diamond lattice the two sublattices are equivalent there is no contribution proportional to σ_z in the interaction matrix and therefore this criterion is always fulfilled, rendering the Luttinger Tisza method exact on this lattice.

Using this method, the spiral surface shown in Fig. 1(c) is obtained. Along the $(q,q,0)$-direction in reciprocal space the energy minimum is found at the ordering vector with

$$q = 2\arccos\left(-\frac{J_1+4J_2+3J_3}{4J_2+8J_3}\right) \tag{S2}$$

for ferromagnetic $J_1 < 0$.

Exchange couplings from DFT. In Table S1 we list the numerical values of the exchange couplings J_1, J_2, J_3, J_4 for $MnSc_2S_4$ obtained from DFT [see also Fig. 1(b)]. The couplings have been calculated for five different values of the Hubbard interaction ranging from $U = 3$ eV to $U = 5$ eV. Also shown is the Curie-Weiss temperature Θ_{CW} for each set of spin interactions. In our PFFRG calculations we use the parameters corresponding to $U = 4.5$ eV since this leads to the best agreement of the Curie-Weiss temperature with the experimental value $\Theta_{CW} = -23$ K.

Temperature evolution of the susceptibility. In addition to Figs. 2 and 3 of the main text, here we present more details of the temperature evolution of the magnetic susceptibility. In Fig. S1 we show the position q of the susceptibility maximum along the line $(q,q,0)$ for $\frac{J_2}{|J_1|} = 1.64$ where $J_3 = 0$ [Fig. S1(a)] and $J_3 = 0.57|J_1|$ [Fig. S1(b)]. Interestingly, while the degree of spiral selection and the width of the spiral surface change considerably with temperature, the peak position along this momentum space direction remains nearly constant, which holds for $J_3 = 0$ and for $J_3 = 0.57|J_1|$. Note that due to the missing J_3 coupling in Fig. S1(a) the calculated maximum position q is considerably larger than the experimentally measured wave vector $2\pi(0.75, 0.75, 0)$ [see also Figs. 1(c) and (d)]. The third neighbor coupling $J_3 = 0.57|J_1|$ shifts the peaks to a position very close to the measured value.

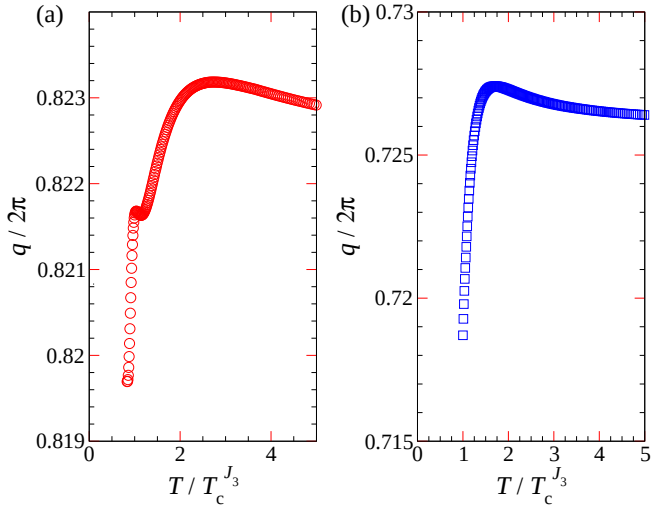

FIG. S1. The evolution with temperature of the wave-vector component q which yields the maxima of the susceptibility along the $(q,q,0)$ direction for the model Hamiltonian with $\frac{J_2}{|J_1|} = 1.64$ and (a) $J_3 = 0$, and (b) $J_3 = 0.57|J_1|$.

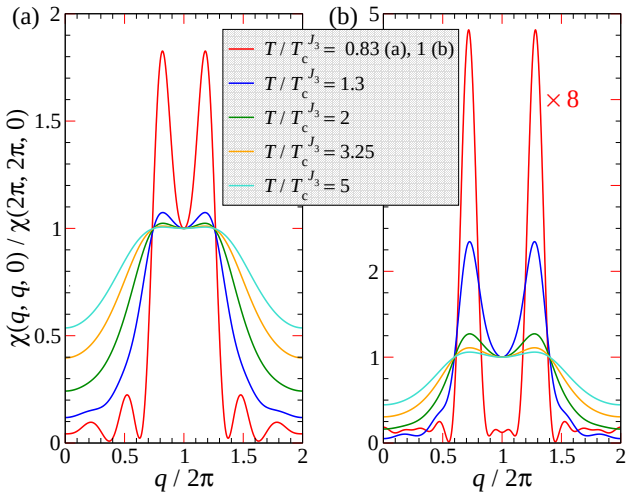

FIG. S2. The variation of the susceptibility (in units of $1/|J_1|$) along a $1D$ cut in the $(q,q,0)$ direction at different temperatures for a model Hamiltonian with $\frac{J_2}{|J_1|} = 1.64$ and (a) $J_3 = 0$, and (b) $J_3 = 0.57|J_1|$.

In Fig. S2 we show the susceptibility along the line $(q,q,0)$ for various different temperatures where the coupling parameters are the same as in Fig. S1. For each plotted temperature the susceptibility is normalized with respect to its value at $(2\pi, 2\pi, 0)$ to compensate for an overall decrease with temperature. Our results for $J_3 = 0$ and for $J_3 = 0.57|J_1|$ both show a clear broadening of the susceptibility along the radial $(q,q,0)$-direction as temperature increases, see also Fig. 3 (the oscillating behavior of the red curves at small susceptibilities is an artifact caused by the finite number of Fourier com-

U (eV)	J_1 (K)	J_2 (K)	J_3 (K)	J_4 (K)	Θ_{CW} (K)
3.0	$-0.465(2)$	1.117(1)	0.364(1)	0.0039(6)	-46
3.5	$-0.433(2)$	0.918(1)	0.305(1)	0.0029(5)	-38
4.0	$-0.404(1)$	0.755(1)	0.257(1)	0.0022(4)	-31
4.5	$\mathbf{-0.378(1)}$	$\mathbf{0.621(1)}$	$\mathbf{0.217(1)}$	$\mathbf{0.0015(3)}$	$\mathbf{-25}$
5.0	$-0.356(1)$	0.509(1)	0.184(1)	0.0009(3)	-20

TABLE S1. Exchange couplings of $MnSc_2S_4$ calculated within GGA+U at $J_{\mathrm{H}} = 0.76$ eV and $6 \times 6 \times 6$ k-points. The parameters corresponding to $U = 4.5$ eV (marked in bold) are used for the PFFRG simulations.

ponents included in our numerics). At small temperatures the susceptibility shows a clear double peak structure, where the peak at smaller q belongs to the spiral surface around $(0, 0, 0)$ and the peak with larger q corresponds to the spiral surface around $(4\pi, 4\pi, 0)$. A pronounced double peak indicates that different spiral surfaces are clearly distinguishable pointing towards an intact spiral spin liquid. As can be seen in Fig. S2, with increasing temperature, the two peaks smear out considerably faster for $J_3 = 0$ as compared to $J_3 = 0.57|J_1|$, implying that a finite J_3 coupling may also stabilize a spiral spin liquid. The most pronounced peak structure is observed for $J_3 = 0.57|J_1|$ close to criticality [red curve in Fig. S2 (b)]. In this case, however, a strong selection of spiral states along the surface takes place [see Fig. 2(f) and Fig. 3] indicating the onset of conventional magnetic order instead of the formation of a spiral spin liquid.